Electrochemistry and Morphology Evolution of Carbon Micro-net Films for Rechargeable Lithium Ion Batteries

ARTICLE *in* THE JOURNAL OF PHYSICAL CHEMISTRY C · AUGUST 2008

Impact Factor: 4.77 · DOI: 10.1021/jp800659n

5 AUTHORS, INCLUDING:

Chilin Li
Chinese Academy of Sciences
37 PUBLICATIONS **630** CITATIONS

SEE PROFILE

Qian Sun
The University of Western Ontario
39 PUBLICATIONS **637** CITATIONS

SEE PROFILE

Electrochemistry and Morphology Evolution of Carbon Micro-net Films for Rechargeable Lithium Ion Batteries

Chi-Lin Li,[†] Qian Sun,[†] Gong-Yu Jiang,[†] Zheng-Wen Fu,*[,†] and Bao-Ming Wang[‡]

Department of Chemistry & Laser Chemistry Institute, Shanghai Key laboratory of Molecular Catalysts and Innovative materials, Fudan University, Shanghai, 200433, P.R.China, and Tianjin Institute of Power Sources, Tianjin, 300381, P. R. China

Received: January 23, 2008; Revised Manuscript Received: April 29, 2008

The highly ordered carbon micro-net films (CMNFs) have been fabricated through patterning and pyrolyzing SU-8 photoresist. They are structurally characterized by transmission electron microscopy and selected area electron diffraction, and they exhibit the mixed phases of both crystalline and disordered carbon. An initial discharge capacity of as large as 350 μAh/cm^2 is observed, and the pseudocapacitance-like charge/discharge curves with reversible capacity of about 100 μAh/cm^2 are shown in the following cycles. From the images of scanning electron microscopy, the originally three-dimensional architecture of CMNFs is well kept after long-term electrochemical cycling. The kinetic parameters such as solid electrolyte interphase resistance, charge transfer resistance, and chemical diffusion coefficients of Li^+ insertion are estimated by alternate-current impedance measurements. The CMNFs are expected to be promising electrodes for future three-dimensional microbatteries.

1. Introduction

Lithium ion microbatteries have emerged as a promising power source for many potential applications in microdevice fields such as radio frequency intelligent cards (RF-ID), on-chip memory, and implantable medical micromachines. In the recent progress, planar all-solid-state thin-film batteries as suggested by Bates et al.[1] have already been in the pilot production stage. For these systems, metal Li and lithium phosphorus oxynitride (LiPON) thin films have been used as anode and solid electrolyte, respectively.[2] However, these two-dimensional (2D) thin-film batteries usually require a quite large active area to provide the adequate capacity and energy. To obtain the small footprints and the large capacity, many three-dimensional (3D) architectures have been put forward.[3]

To achieve high-performance 3D lithium ion batteries, it is crucial to search for easily fabricated 3D electrode materials with large capacity. Carbon-based materials have been widely studied as anodes for a long-term and exhibited many advantages such as low cost, excellent thermal and chemical stability, environmental friendliness, and easy preparation in various forms. Apart from graphite,[4] disorded and amorphous carbon,[5] carbon nanotubes,[6,7] and nanofibers,[8] which have been thoroughly investigated in traditional batteries, the carbon micro-electromechanical systems (C-MEMS) have recently been considered as 3D electrodes for 3D microbatteries.[9] In the reported C-MEMS, high-aspect-ratio carbon column arrays showed the primary electrochemistry in nonaqueous electrolyte.[9,10] However, one question of whether these carbon arrays with regular shape could be well maintained after long-term electrochemical cycling and reaction with Li^+ still remains unknown. The clarification of how Li^+ intercalates into C-MEMS frameworks is very important not only for searching for the best fabrication conditions, but also for the feasibility analysis of raw photoresist materials for future 3D microbatteries.

In this case, another 3D material of C-MEMS, called carbon micro-net films (CMNFs) is expected as anode for the potential application in such a 3D battery prototype, where the solid electrolyte and cathode can be deposited in succession by some special methods, such as low pressure chemical vapor deposition (LPCVD),[11] on the micrometric net walls of CMNFs. On the other hand, unlike carbon microcolumn arrays, the CMNF itself can also be used as current collectors because of the network continuity. This will simplify the C-MEMS fabrication technology, and the preparation of current collector layers for CMNFs could be removed. For this work, we investigate the electrochemical performance for CMNFs and the possible pathway of Li^+ insertion into CMNFs in nonaqueous liquid electrolyte. This Li^+ moving pathway can be well discerned from the shape evolution of this 3D material under its reaction with Li^+ and electrolyte penetration effect. These results will provide significant guidance to optimize the 3D CMNFs with better fabrication parameters and larger active area in the future works on C-MEMS and 3D solid microbatteries.

2. Experimental Section

The fabrication of CMNFs is similar to the previous C-MEMS manufacture process for high aspect ratio carbon posts suggested by Wang[9] and consists of two stages: patterning the photoresist by photolithography and pyrolyzing the patterned photoresist. At first, the SU-8 was used as the photoresist, which was uniformly spin-coated on a SiO_2-grown Si substrate. Then, masks were designed to form microstructural networks with four square holes, which exhibited a width and depth of about 16 and 8 μm, respectively, and the side width of micronet films between two holes was about 8 μm. Some steps such as spin coating, soft bake, near UV exposure, development, and postbake were involved in this photolithography using SU-8 photoresist. In the next stage, the patterned SU-8 films were

* Corresponding author phone: +86-21-65642522; e-mail: zhengwen@sh163.net.
[†] Fudan University.
[‡] Tianjin Institute of Power Sources.

10.1021/jp800659n CCC: $40.75
Published on Web 08/12/2008

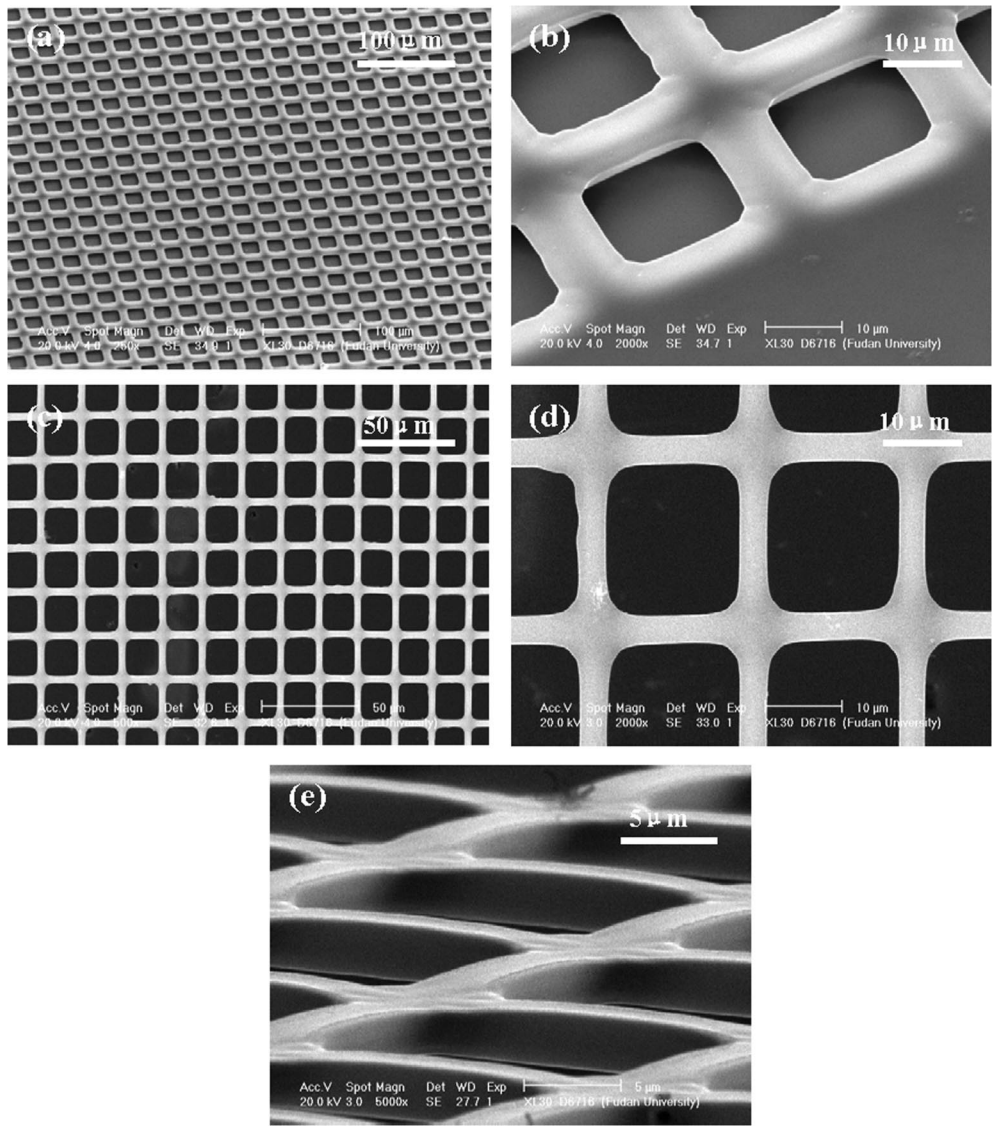

Figure 1. SEM images of (a−b) patterned SU-8 photoresist films and (c−e) as-fabricated CMNFs.

pyrolyzed at high temperature and oxygen-free ambience. In a quartz-tube furnace, the samples were heated in N_2 atmosphere at 300 °C for 40 min first. Then, the temperature was increased at a rate of 10 °C per minute to 900 °C in the N_2 flux of 2000 standard cm^3 min^{-1} (sccm). Next, the samples were kept at 900 °C for 1 h in 5% H_2 mixed N_2 gas at a rate of 2000 sccm. Finally, the heat source was turned off, and these samples were cooled to room temperature in a pure N_2 atmosphere.

The surface and cross-section morphologies with different scales of patterned SU-8 films and as-fabricated CMNFs were investigated by scanning electron microscopy (SEM) (Cambridge S-360). The structure and crystallinity of as-fabricated CMNFs were characterized by high resolution transmission electron microscopy (HRTEM) and selected area electron diffraction (SAED) measurements, which were carried out by a 200 kV side entry JEOL 2010 TEM. For electrochemical detection, a conventional three-electrode cell was equipped with the CMNFs as the working electrode and two high-purity lithium foils as the counter electrode and reference electrode, respectively. The electrolyte consisted of 1 M $LiClO_4$ in a nonaqueous solution of ethylene carbonate (EC) and dimethyl carbonate (DMC) with a weight ratio of 1:1 (Merck). The cells were assembled in an Ar-filled glovebox. Charge−discharge measurements were performed at room temperature with a Land BT 1−40 battery test system. The cells were cycled between 0 and 3 V versus Li/Li^+ at a current density of 6 $\mu A/cm^2$. For the ex situ measurements of SEM for electrochemically cycled CMNFs, the samples after charging or discharging were disassembled in the Ar-filled glovebox for avoiding the exposure to oxygen or water and were rinsed by anhydrous DMC to eliminate residual salts. Cycle voltammogram (CV) and alternate-current (AC) impedance measurements were carried out in a CHI 660a electrochemical working station (CHI Instruments). A scanning rate of 0.2 mV/s was implemented in CV measurement over a potential range between 0 and 3.2 V. The AC impedance spectroscopy of cells measured at different charge/discharge potentials was carried out in the frequency region of 0.05−100 kHz and then simulated and analyzed by the software Autolab-FRA (Version 4.9).

3. Results and Discussion

It has been demonstrated that SU-8 photoresist could produce high-quality carbon microarrays with a variety of complex structures;[12] also, it is expected to form ordered CMNFs through patterning and pyrolysis. Figure 1 exhibit the SEM images of patterned SU-8 films (Figure 1, panels a and b) and the as-fabricated CMNFs (Figure 1, panels c−e), respectively, in a

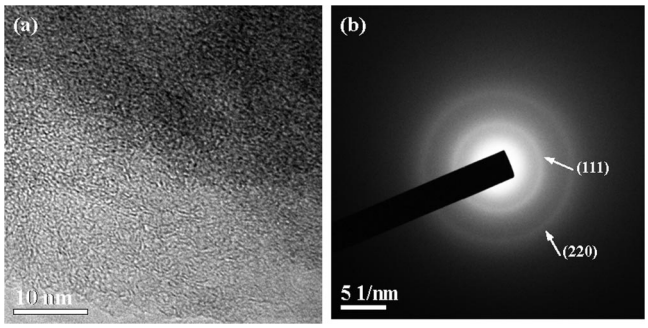

Figure 2. (a) High resolution TEM image and (b) SAED pattern of as-fabricated CMNFs.

variety of scales. It can be observed that the CMNFs maintain well-ordered shape and 3D architecture as patterned photoresist before pyrolysis. In addition, it should be noted that the sides of CMNFs are greatly shrunk as compared with precursor SU-8 pattern, and merely half of the size of SU-8 samples (shown in Figure 1, panels c−e). The degree of shrinkage in the respective direction during the formation of CMNFs is quite uniform, and both the width and depth of the microscopic sides for CMNFs are about 4 μm.

From the TEM image and SAED pattern of as-fabricated CMNFs shown in Figure 2, the diffraction rings representing face-centered cubic structure are observed to be weak, moreover wide, whereas some short moiré stripes could be locally found. It indicates that the CMNFs are not structurally well ordered, and some diamond-like crystalline phases should exist in the amorphous carbon matrix. It is of great possibility that the photoresist-derived pyrolytic carbon films usually show the mixed feature of crystalline and disordered structures, which has also been detected in carbon films fabricated from other photoresist precursor such as AZ 4330.[13] According to the suggestion by Dahn et al. that disordered carbon could store more lithium than graphite,[14] the capacity of disordered CMNFs are expected to exceed the theoretical value of graphite.

The electrochemical reaction performance of CMNFs with metal lithium is shown in Figure 3. From the CV curves shown in Figure 3a, the redox peaks are far from good symmetry and show a complex electrode reaction process. During the first reduction process, two main CV peaks can be seen in the low potential ranges around 0.7 and 0.3 V, respectively. Moreover, these peaks are much more pronounced than the ones shown in the following reduction stages. For the next two cycles, two main reductive peaks are repeatedly shown at 0.8 and 0.0 V. In contrast, no apparent oxidative peaks can be observed during the first three cycles. These redox peaks in the CV curves imply the existence of various Li sites in CMNFs and intermediate Li-inserted carbonous materials, the details of which still remain unknown.

The charge/discharge properties of CMNFs shown in Figure 3b are in good agreement with the CV results. Evidently, the first discharge capacity for CMNFs is as high as 350 μAh/cm^2, and the large initial irreversibility, which is the characteristic of disordered carbon, can be observed. The following electrochemical behavior and cycling stability are well maintained (shown in Figure 3c), and the reversible capacity is kept at about 100 μAh/cm^2 within 100 cycles. It is proved that the long cycleablility can be obtained from SU-8 derived carbonous materials. Considering the potential application in 3D microbatteries, this area ratio capacity of CMNFs is high enough to guarantee the normal work for many microelectronic devices, such as on-chip RF-ID, and is comparable with the capacity of

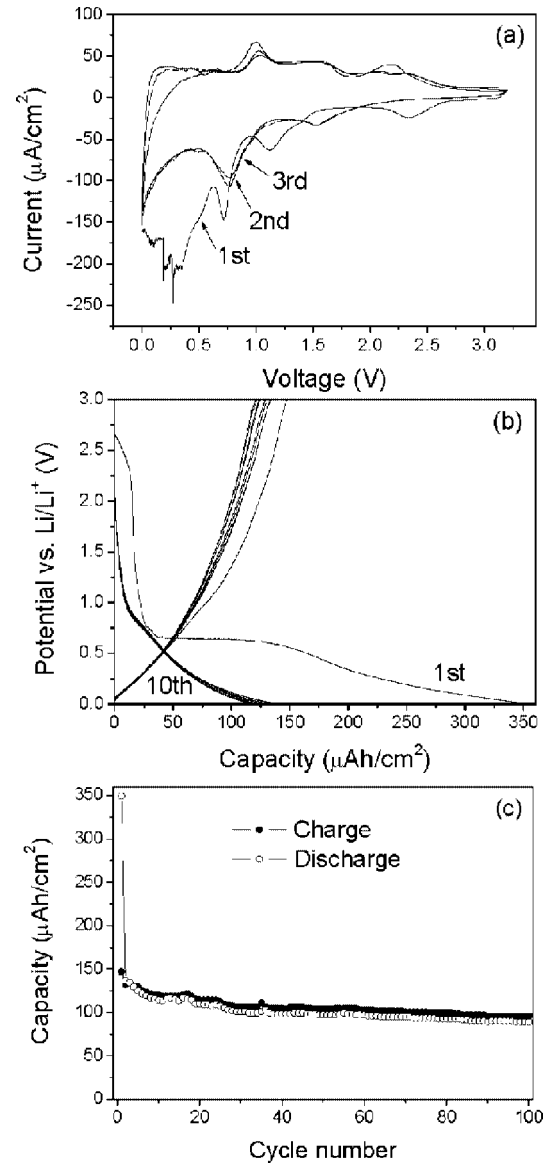

Figure 3. (a) Cyclic voltammograms of CMNFs for the first three cycles in a potential range of 0−3.2 V with a constant scanning rate of 0.2 mV/s. (b) Potential profiles vs capacity, and (c) charge/discharge capacity as a function of cycle number of CMNFs in a voltage range of 0−3 V with a constant current density of 6 μA/cm^2.

carbon micropost arrays fabricated from the same photoresist.[9] Moreover, it can be apparently seen that the capacity is mostly localized in the potential region of 0.0−1.0 V with the pseudocapacitance-like charge/discharge curves. This is in great difference from some traditional and well-crystallized carbon materials, such as graphite carbons[4] and graphitized mesocarbon microbeads,[15] which exhibit distinct reactive plateaus at a lower voltage range of 0.0−0.2 V. In fact, it has been demonstrated that disordered or nanosized carbon materials always present steep charge/discharge curves with the absence of distinct voltage plateaus,[6,16,17] indicating a different Li storage mechanism from layered graphitized carbon, which presents a staging mechanism via well-defined interstitial sites. Additionally, according to other results,[18] the large initial irreversibility for CMNFs could be associated with electrolyte reduction and formation of a solid electrolyte interphase (SEI) on the CMNF surface, which are not expected to occur in the following cycles. The long distinct plateau at 0.6−0.7 V, which is only observed in the first discharge, should be attributed to the formation of the ionically conducting SEI.

As it has been seen, the SU-8 photoresist is a precursor material that is suitable for the preparation of a variety of 3D patterned C-MEMS, such as posts, wires, bridges, and plates, through controlling the processing parameters and heating conditions.[12] As another prototype derived from SU-8, our CMNFs show the similar Li^+ insertion behavior as other CMEMS from the CV and charge/discharge results. It indicates that the Li-inserted electrochemistry is certainly determined by the intrinsic property of pyrolyzed SU-8 rather than the styles of 3D design. On the other hand, it is not yet known whether these microstructural 3D samples with various patterns are robust enough as electrodes in nonaqueous liquid electrolyte, and their original morphology can be well kept after long-term electrochemical cycles. It should be mentioned, once these carbonous 3D architectures are demonstrated to be electrochemically stable in liquid electrolyte, that the structural integrity under all-solid-state environment should be expected to be better due to a much more favorable electrode−electrolyte interface. In our work, the galvanostatic performance shown in Figure 3, panels b and c, is considered to be associated with structural integrity, morphology evolution, and Li^+ reaction pathway of 3D electrodes, which will be discussed according to the SEM images of cycled CMNFs. These results can also provide hints as to whether pyrolyzed SU-8 photoresist patterns can be orderedly maintained under the soakage of liquid electrolyte.

Here, the SEM images of different cycling stages and corresponding Li^+ insertion models are shown in Figure 4. After the first discharge, as shown in Figure 4a, no great morphology change for CMNFs can be found, but the sides of this carbon network become much rougher as compared with uncycled samples. The unavoidable surface defects arisen during pyrolysis process may favor Li^+ insertion and adsorption in CMNFs. The coarsened and widened sides of CMNFs show the trace of Li^+ adsorption and SEI formation on CMNF's surface. From the initial noncapacitance-like discharge behavior, apart from the Li^+ ions, which occupy the surface sites, other Li^+ ions are likely to enter into the inner of CMNFs. However, the question of how Li^+ ion intercalates into the CMNF's remains unknown so far. In a liquid electrolyte environment, it should be convinced that the Li^+ moving path within CMNFs could be discerned after enough cycles due to the effect of electrolyte penetration.

From the SEM morphology of CMNFs after 100 cycles, as shown in Figure 4b, this distinct pattern is still well kept, and it is in agreement with the good electrochemical cycleability. Unlike the nanosized tubes and fibers,[6] where Li ions intercalate into the intrinsic channels, disrupt the intertube binding, and lead to the deterioration of original structure, the CMNFs are quite robust without the presence of microside's distortion and rupture under long-term electrolyte penetration and Li^+ attack. From the standpoints for the mechanical stability and possible application in commercial 3D batteries, the architecture stability implies the advantage of a micrometric network over nanometric structures. However, it should be noted, if comparing Figure 4, panels a and b, that the sides of CMNFs are extended but are narrowed to some degree with the grid increasing within the network structure. Combined with the reaction model of CMNFs (shown in Figure 4c), a reasonable Li^+ insertion mechanism is suggested. As observed, the pathway of Li^+ moving is almost parallel to the cross section of CMNFs, indicating most Li^+ sites are localized on the planar position, which is vertical to the direction of principal axis of CMNF sides. This kind of reactive mechanism is expected to modify the intrinsic structure of CMNFs and to facilitate the lengthways extension and transverse shrinkage of every side.

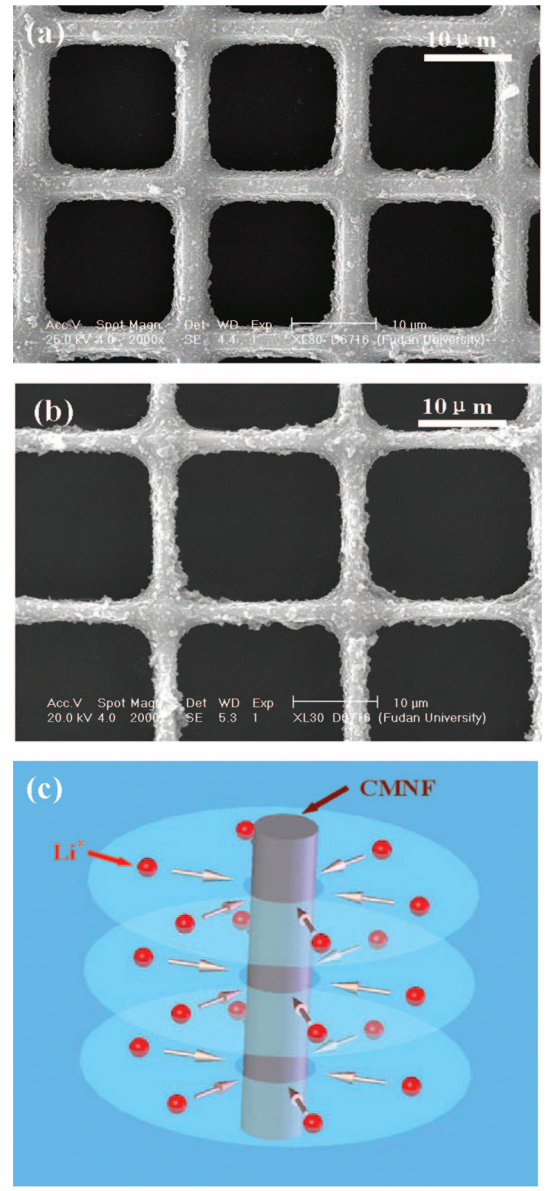

Figure 4. SEM images of CMNFs fabricated under the absence of pyrolysis temperature gradients after (a) the 1st discharge and (b) the 100th cycle between 0 and 3 V at a current density of 6 $\mu A/cm^2$, respectively. (c) Corresponding reaction model of CMNFs with Li^+.

Surprisingly, another Li^+ insertion phenomenon after the 100th cycle can be seen for the same group of samples, which are put at the edge of the tube furnace during the pyrolysis process. The SEM images and corresponding reaction model for such samples are presented in Figure 5. It is observed that the CMNFs after long-term electrochemical reaction show evident morphology evolution and look like willow leaves, as their sides are cleft into several narrower microsticks around the principal axis. According to the reaction model, it is imaginable that the Li^+ insertion sites are mostly congregated along the axis line of the sices of CMNF; thus, the direction of Li^+ insertion is mainly vertical to the cross section of CMNFs. Because of the fixed nodes in CMNFs, the cleft branches with smaller size are pushed outward a little but are still gathered together to maintain the network structure. The observed interspaces among branches could reduce the electronic connect of electrodes. Therefore, it is understandable that these samples show faster electrochemical degradation (not presented here) as compared with the samples pyrolyzed in the center of the

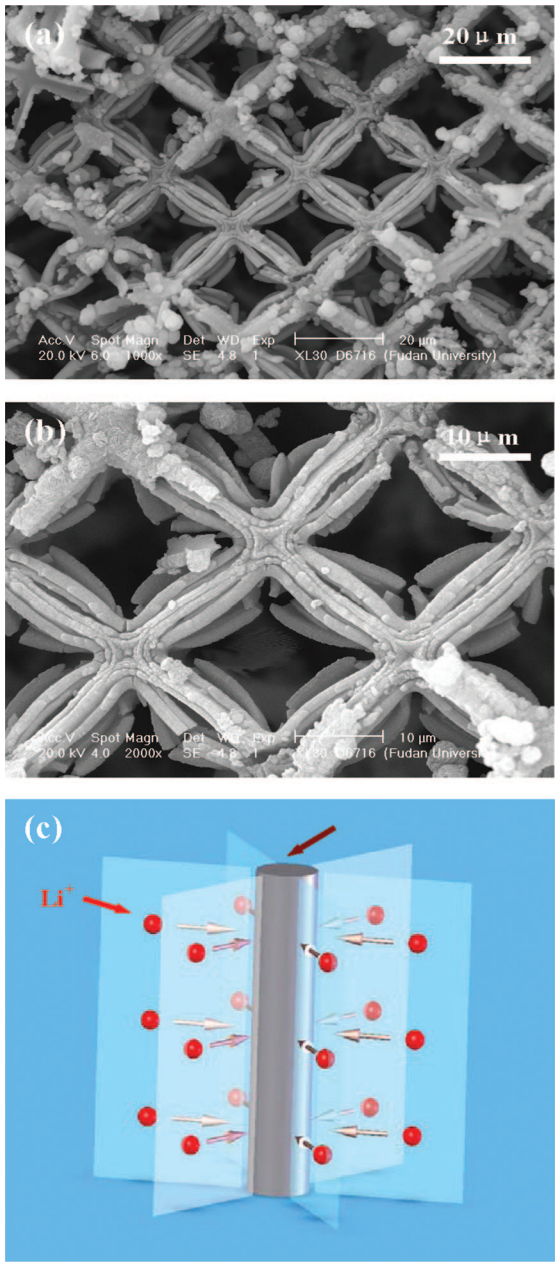

Figure 5. (a) SEM image and (b) enlarged SEM image of CMNFs fabricated under the presence of great pyrolysis temperature gradients after the 100th cycle between 0 and 3 V at a current density of 6 μA/cm^2. (c) Corresponding reaction model of CMNFs with Li^+.

tube furnace. The pyrolysis position of CMNF samples in the tube furnace and the resultant difference in temperature gradients should be associated with the diversity of the intrinsic texture and Li^+ insertion position, which consequently results in the difference in the Li^+ moving pathway in CMNF inner and electrochemistry. It means that the fabrication parameters for high-quality CMNFs should be strictly investigated and controlled. The large temperature gradients should be avoided in preparation. In addition, it should be noted that, despite the occurrence of structural separation under unfavorable pyrolysis conditions, the continuity of network structure and fixing of nodes can guarantee the mechanical integrity of the original pattern and result in a variety of interestingly regular morphologies. Therefore, as an anode material for 3D batteries, the 3D CMNFs are expected to be a better choice than other C-MEMS, such as carbon post arrays, in the aspects of morphological modification, structural controlling, and mechanical stability.

To obtain the kinetic information of CMNFs during the reversible discharge stage, AC impedance is used to investigate the various resistance changes and Li^+ insertion diffusion coefficients. The Nyquist plots of CMNFs at various reaction potentials from 1.4 to 0.0 V are shown in Figure 6a, after the electrode has been cycled three times. The testing potentials are obtained from the method of bulk electrolysis coulometry. Most of the impedance responses exhibit partly overlapped semicircles at high and intermediate frequencies, followed by a sloping line at low frequencies. As is known, the SEI and charge-transfer-dominated regimes are reflected at high and intermediate frequencies, respectively, and in the range of low frequencies, diffusion of charge in CMNFs is the dominant factor.[19] Combined with the physical−chemical properties of our system and the suggestion by Mohamedi et al.,[20] a suitable equivalent circuit model is proposed in Figure 6b, and least-squares fitting is used to simulate the measured impedance spectra. There are 10 kinetic parameters resulting from 7 circuit elements mentioned in this model. The circuit consist of a bulk electrolyte resistance (R_e), a SEI layer resistance (R_{SEI}), a charge transfer resistance (R_{ct}), two constant phase elements (CPE_1 and CPE_2), a semi-infinite Warburg impedance (Z_w) describing the solid-state diffusion of Li^+ in low frequencies, and a finite-space Warburg impedance (Z_{FSW}) describing both diffusion and accumulation of Li^+ at very low frequencies. It should be noted that, considering the defective and inhomogeneous natures of CMNF electrodes, the ideal double-layer and SEI layer capacitances (C_{dl} and C_{SEI}) are replaced by their respective CPEs due to the deviation from an ideal system in our case.[21,22] The impedance of CPE is defined as $Z = (1/Y_0)(jw)^{-n}$, where $j = (-1)^{1/2}$, w is the angular frequency, and Y_0 and n are constants. The CPE becomes an ideal capacitance (C) when $n = 1$ and, hence, $Y_0 = C$.

The change of three resistance parameters (R_e, R_{SEI}, and R_{ct}) obtained from the simulation of impedance spectra, according to the circuit model described above, is shown in Figure 6c. It can be observed that the bulk electrolyte resistance (R_e) exhibits the lowest value and is almost independent of the applied potentials. For SEI layer resistance (R_{SEI}), along with the drop of potentials, the resistance values monotonously decrease as well, indicating the SEI layers on CMNF surface become thinner at lower potential. Perhaps the electric field distortion induced by electrode structure is another reason for the R_{SEI} variation, because this could create local concentration gradients within the porous parts of the SEI layer. In contrast, the charge transfer resistance (R_{ct}) exhibits the opposite increase tendency with the deepening of discharge process. On the basis of the hypothesis that SEI is thinner for lower potentials and thicker for higher potentials, it implies that the ionic conductive SEI formation is favorable for the charge-transfer kinetics. The resistance results are in disagreement with the impedance data of carbon micropost array electrodes, where the R_{SEI} and R_{ct} showed the reverse change tendency.[10] The impedance discrepancy may be related with the geometries of various kinds of CMEMS.

Other kinetic parameters estimated from the AC impedance spectra in various reaction potentials are shown in Table 1. The parameter n values shown in CPE_1 and CPE_2 should be associated with the degree of inhomogeneity in SEI layers and charge transfer regions, respectively.[21,22] The n value of CPE_1 lies in the value range of 0.48−0.57, which is much less than 1 and the n value of CPE_2, which is in the range of 0.70−0.93. The relatively low n value in CPE_1 reflects the rough electrode surface covered by SEI layers, which can be apparently observed in the SEM images of cycled CMNFs (shown in Figure 4, panels

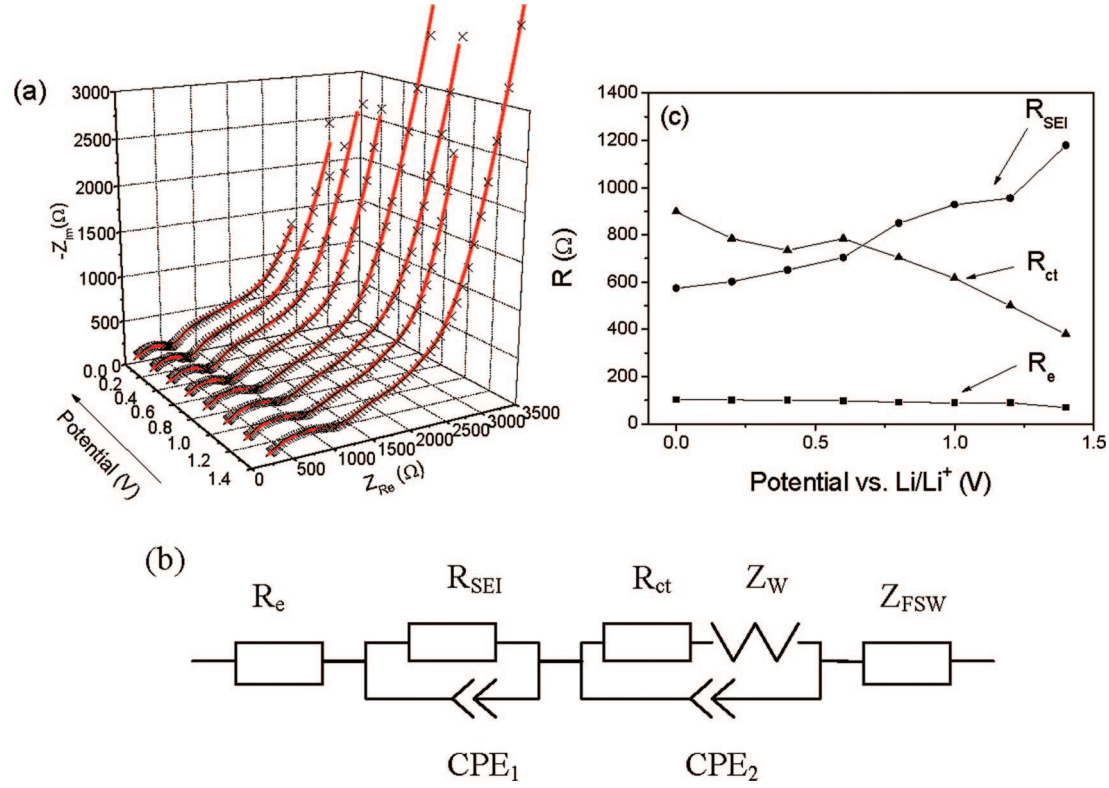

Figure 6. (a) Nyquist plots of CMNFs at different discharge stages from 1.4 to 0 V with a step of 0.2 V after three cycles; (black, ×××) experimental plots and (red, —) simulating curves. (b) Equivalent circuit model used for least-squares fitting of Nyquist plots. (c) Plots of various simulated resistances vs potential at different discharge states.

TABLE 1: Values of the Circuit Model Parameters for the Fit to Impedance Data of CMNFs at Different Discharge State

				CPE_1			CPE_2		Z_W Z_{FSW}	
discharge potentials (V)	R_e (Ω)	R_{SEI} (Ω)	Y_0 (× 10^{10}) ($\Omega^{-1}s^{0.5}$)	n	R_{ct} (Ω)	Y_0 (× 10^5) ($\Omega^{-1}s^{0.5}$)	n	Y_0 (× 10^4) ($\Omega^{-1}s^{0.5}$)	Y_0 (× 10^4) (Ω^{-1} $s^{0.5}$)	B ($s^{0.5}$)
1.4	69.3	1180	0.26	0.48	379	1.41	0.93	7.61	7.74	1.05
1.2	89.2	956	1.05	0.53	500	0.45	0.81	9.38	7.10	1.17
1.0	88.7	928	1.03	0.53	617	0.25	0.76	8.08	9.37	1.18
0.8	91.5	850	1.76	0.55	704	0.17	0.71	8.92	11.38	1.17
0.6	97.4	704	2.69	0.56	784	0.19	0.70	11.03	13.04	1.37
0.4	99.9	651	3.73	0.57	734	0.41	0.76	11.73	15.06	1.50
0.2	101.7	602	4.87	0.57	784	0.37	0.75	12.14	18.74	1.57
0.0	102.4	574	5.15	0.57	898	0.26	0.73	12.35	26.67	1.73

a and b). In addition, the n value of CPE_1 gradually increases along with the discharge process. If SEI is thinner for lower potentials and thicker for higher potentials as mentioned above, then the n value increase in CPE_1 is accorded with the attenuation of SEI layers, which could result in a smoother electrode surface at a lower potential. For determination of the chemical diffusion coefficient (D_{Li}) of Li^+ into CMNFs at certain discharge potentials, finite-space Warburg impedance (Z_{FSW}) is analyzed according to our impedance model. According to the description of Boukamp, ZFSW is given by eq 1.[23]

$$Z_{FSW} = (1/Y_0)(jw)^{-1/2} \coth[B(jw)^{1/2}]$$

Here, $B = L/D_{Li}^{1/2}$ is the diffusion constant, and L is the diffusion layer thickness. In this case, the electrolyte is expected to penetrate the whole structure and enable a good wetting of the surface from the SEM of cycled electrodes. Therefore, half of the depth of the CMNF side as diffusion layer thickness is assumed. Therefore, the D_{Li} values at various potentials could be calculated from the simulated constant B and are in the range of 1.34 × 10^{-8} to 3.63 × 10^{-8} cm^2/s, which implies the high-rate diffusion of Li^+ into CMNFs. Moreover, with more Li^+ insertion in CMNFs, the diffusion coefficient becomes relatively smaller and is in good agreement with the conclusion of larger charge transfer resistance at lower potential.

4. Conclusions

The 3D CMNFs as a prototype of CMEMS have been successfully fabricated by micro- machining technology, consisting of SU-8 photoresist patterning by photolithography and a two-step pyrolysis process. They structurally present the short-distance ordered diamond-like phases, which exist in the amorphous carbon matrix. The first discharge capacity for CMNFs is calculated to be as high as 350 $\mu Ah/cm^2$, part of which can be ascribed to the irreversible formation of SEI layers. The reversible capacity in the subsequently long-term cycles is well maintained at about 100 $\mu Ah/cm^2$. The pseudocapacitance-like electrochemical behavior and wide CV redox peaks indicate complex electrode reaction with Li^+ as compared with graphitized carbonous materials. After the 100th cycle, the original 3D shape of CMNFs is well kept without the presence of

structural collapse and network rupture. A reasonable Li^+ moving pathway is concluded according to the size self-regulation of the CMNF pattern under the effect of electrolyte penetration. Under the absence of pyrolysis temperature gradients, most of Li^+ can be intercalated or deintercalated paralleling to the cross-section of CMNF sides. The AC impedance spectra and corresponding circuit model detailedly reflect the results of SEI change, charge transfer, and Li^+ diffusion kinetics along with more Li^+ insertion. Due to the features of both the continuity of network structure and fixing of nodes, the CMNFs are expected to provide some interesting information, such as controlled morphological modification under structural integrity and Li^+ reaction paths in electrodes. For achieving satisfactory Li-insertion performance, the homogeneous pyrolysis temperature of photoresist is demonstrated to be necessary. As 3D electrode material, they can be aimed for promising application in future commercial 3D solid microbatteries.

Acknowledgment. This work was supported by the National Nature Science Foundation of China (Project No. 20773031), 973 Projects (2007CB209702), and 863 Projects (2007AA03Z322)

References and Notes

(1) Bates, J. B.; Dudney, N. J.; Neudecker, B.; Ueda, A.; Evans, C. D. *Solid State Ionics* **2000**, *33*, 135.

(2) Li, C. L.; Fu, Z. W. *Electrochim. Acta* **2007**, *52*, 6155.

(3) Long, J. W.; Dunn, B.; Rolison, D. R.; White, H. S. *Chem. Rev.* **2004**, *104*, 4463.

(4) Chang, Y. C.; Sohn, H. J. *J. Electrochem. Soc.* **2000**, *147*, 50.

(5) Gnanaraj, J. S.; Levi, M. D.; Levi, E.; Salitra, G.; Aurbach, D.; Fischer, J. E.; Claye, A. *J. Electrochem. Soc.* **2001**, *148*, A525.

(6) Claye, A. S.; Fischer, J. E.; Huffman, C. B.; Rinzler, A. G.; Smalley, R. E. *J. Electrochem. Soc.* **2000**, *147*, 2845.

(7) Frackowiak, E.; Gautier, S.; Gaucher, H.; Bonnamy, S.; Beguin, F. *Carbon* **1999**, *37*, 61.

(8) Subramanian, V.; Zhu, H. W.; Wei, B. Q. *J. Phys. Chem. B* **2006**, *110*, 7178.

(9) Wang, C. L.; Taherabadi, L.; Jia, G. Y.; Madou, M.; Yeh, Y. T.; Dunn, B. *Electrochem. Solid-State Lett.* **2004**, *7*, A435.

(10) Galobardes, F.; Wang, C.; Madou, M. *Diamond Relat. Mater.* **2006**, *15*, 1930.

(11) Notten, P. H. L.; Roozeboom, F.; Niessen, R. A. H.; Baggetto, L. *Adv. Mater.* **2007**, *24*, 4564.

(12) Wang, C. L.; Jia, G. Y.; Taherabadi, L. H.; Madou, M. J. *J. Microelectromech. Syst.* **2005**, *14*, 348.

(13) Ranganathan, S.; McCreery, R.; Majji, S. M.; Madou, M. *J. Electrochem. Soc.* **2000**, *147*, 277.

(14) Dahn, J. R.; Zheng, T.; Liu, Y. H.; Xue, J. S. *Science* **1995**, *270*, 590.

(15) Yao, J.; Wang, G. X.; Ahn, J. H.; Liu, H. K.; Dou, S. X. *J. Power Sources* **2003**, *114*, 292.

(16) Yang, Z. H.; Wu, H. Q. *Mater. Lett.* **2001**, *50*, 108.

(17) Li, N. C.; Mitchell, D. T.; Lee, K. P.; Martin, C. R. *J. Electrochem. Soc.* **2003**, *150*, A979.

(18) Hu, Y. S; Adelhelm, P.; Smarsly, B. M.; Hore, S.; Antonietti, M.; Maier, J *Adv. Funct. Mater.* **2007**, *17*, 1873.

(19) Ho, C.; Raistrick, I. D.; Huggins, R. A. *J. Electrochem. Soc.* **1980**, *127*, 343.

(20) Mohamedi, M.; Takahashi, D.; Uchiyama, T.; Itoh, T.; Nishizawa, M.; Uchida, I. *J. Power Sources* **2001**, *93*, 93.

(21) Striebel, K. A.; Sakai, E.; Cairns, E. J. *J. Electrochem. Soc.* **2002**, *149*, A61.

(22) Shaju, K. M.; Rao, G. V. S.; Chowdari, B. V. R. *J. Electrochem. Soc.* **2004**, *151*, A1324.

(23) BoukampB. A. *Equivalent Circuit Users Manual*; University of Twente:1989.

JP800659N